CHAPTER ONE

Lipid and Membrane Dynamics in Biological Tissues—Infrared Spectroscopic Studies

Satoshi Yoshida[1,*] *and* Kenzo Koike[2]

Contents

Abstract

Functions of cell bilayer membranes are closely linked to dynamics and behavior of network of membrane components including lipids, proteins, and glycans. It is important to investigate the role of membrane components in the membrane functions without damage of the network of components. This is the reason why noninvasive and nondestructive analyses are so important for the study of the

* Corresponding author: Tel./Fax: +81 58 293 2655.
E-mail address: xyosida@gifu-u.ac.jp

[1] Gifu University, Gifu, Japan
[2] Beauty Research Center, Kao Corporation, Tokyo, Japan

Advances in Planar Lipid Bilayers and Liposomes, Volume 13
ISSN 1554-4516, DOI: 10.1016/B978-0-12-387721-5.00001-8

intact membranes and tissues. Vibrational spectroscopies including near- and mid-infrared absorption and resonance Raman scattering spectroscopies are useful for these purposes. In this chapter, we summarize the application of infrared spectroscopy to studies of lipids and bilayer membrane dynamics in biological tissues, and to the research for diagnosis of human diseases.

Abbreviations

18-MEA	18-methyl-eicosanoic acid
AGEs	advanced glycation end products
ATR	attenuated total reflectance
CERs	ceramides
CHOL	cholesterol
DEPE	1,2-dielaidoyl-*sn*-glycero-3-phospho-ethanolamine
DHA	docosahexaenoic acid
DMPA	1,2-dimyristoyl-*sn*-glycero-3-phosphate sodium salt
DPPC	dipalmitoylphosphatidylcholine
ESG	esterified sterylglucoside
ESI-MS	electrospray ionization-mass spectrometry
FFA	free fatty acid
FTIR	Fourier-transform infrared
GAGs	glycosaminoglycans
GalCer	galactocerebroside
GlcNAc	*N*-acetylglucosamine
HDL	high-density lipoprotein
IR	infrared
LDL	low-density lipoprotein
MALDI-TOF-MS	matrix-assisted laser desorption ionization time-of-flight mass spectrometry
NMF	natural moisturizer factor
NMR	nuclear magnetic resonance
PCA	principal component analysis
PLS	partial least square
POPC	palmitoleic phosphatidylcholine
SC	stratum corneum

1. Introduction

Cell membrane and tissue lipid dynamics are playing important roles in the life of all organisms on the earth. Especially, the cell membranes with phospholipid bilayer have mainly two functions (1) clear separation of the

inner cell space from the outer world and (2) mediation of signal transduction and communications between the inner and outer spaces. These important functions of cell membranes are based on various biomolecular components, such as lipids (including fatty acids), proteins (enzymes, receptors, transporters, channels, and cytoskeletons), and glycans, and their interactions.

Functions of cell membranes are closely linked with dynamics and behavior of network of membrane components, such as lipids, proteins, and glycans with the aid of minerals and other nutrients. Thus, it is important to investigate the role of membrane components in the membrane functions without disruption of membrane integrity and without damage of the network of components. This is the reason why noninvasive and nondestructive analyses are so important for the study of membrane components in the intact membranes.

For noninvasive and nondestructive analyses of membrane systems, vibrational spectroscopies including near- and mid-infrared absorption and resonance Raman scattering spectroscopies are useful for these purposes. Vibrational spectroscopy can reveal the characteristics and interaction with the environment of biomolecules. Basically, the mid-infrared spectroscopy is based on the net changes of dipole moment of the molecules ("IR-active"), whereas the Raman spectroscopy is based on the change of electric polarizability of the molecules ("Raman-active"), and thus these spectroscopies are complementary techniques for studies in chemistry.

The mid-infrared absorption and Raman scattering spectroscopies are frequently used to study the interaction between lipids and proteins or glycans in the cell membrane, and this is due to the evidence that the energy level of hydrogen bonding or some interactions is comparable to the infrared energy level, and the interaction change between functional groups of membrane biomolecules (e.g., receptors, channels, glycoproteins, and glycolipids) and the surrounding water or lipid or protein molecules may be detectable in the infrared region.

Vibrational spectroscopy can reveal not only the characteristics of specific functional group, but also the mixture of many functional groups. As a matter of fact, the change of membrane dynamics may be in part the result of change of biomolecular networks in the membrane. This is because the application of statistical multivariate analysis or chemometrics to vibrational spectroscopy is useful and important for the noninvasive analyses of cell membranes, food staffs, and human tissues.

In the multivariate analysis or chemometrics for vibrational spectroscopy, the principal component analysis (PCA) and partial least square (PLS) regression analysis methods are frequently used for classification or categorization of phenomena, such as membrane dysfunction, or predication of change of factors which are, for example, some disease-related lipids and fatty acids. These statistical methods may provide vibrational

spectroscopy—the chance to supersede the diagnosis of diseases with invasive clinical tests and destructive tests of food staffs.

The vibrational spectroscopy has been widely applied to the diagnostic analysis of diseases and nondestructive analysis of food staffs; however, at present there have been few vibrational spectroscopic techniques used as golden standard methods for diagnostic analyses. Usually biochemical analyses of blood or other body fluids have been used for the diagnosis as standard methods, and only one or a few specific factors could be measured in one shot of detection. For example, total cholesterol (CHOL), LDL, HDL, and triglycerides were mainly measured for diagnosis of hyperlipidemia which would be linked, in some cases, to complex metabolic diseases. Some complex diseases such as diabetic diseases and atherosclerosis may have complex pathogenic mechanisms with many onset factors and thus many biomarkers.

To realize those complex diseases and diagnosis, the technique which would detect many factors in a short time noninvasively by one shot of measurement would be very useful, and for this purpose the vibrational spectroscopy—especially mid-infrared spectroscopy—would be suitable because it can detect the change of properties of cell bilayer membranes including proteins, lipids, and glycans simultaneously, and actually the near- and mid-infrared spectroscopy as well as Raman scattering spectroscopy may have a great potential in the clinical diagnostics field.

In this chapter, we summarize the advances of infrared spectroscopic techniques in the study of cell membranes and lipids and their interactions with other biomolecules in relation to the diagnosis of human diseases.

2. Historical View of Vibrational Spectroscopic Studies on Lipids and Membrane Dynamics in Biological Tissues

Application of vibrational spectroscopy, especially mid-infrared spectroscopy, to the studies of cell membrane and lipids has a long history and has provided a lot of data concerning to the study of membrane and lipid dynamics in human tissues.

2.1. Membrane Fluidity

Infrared spectroscopy could reveal the fluidity change of the cell membranes and liposomes with measuring the methylene CH stretching mode of the membrane fatty acyl chains [1,2]. Membrane fluidity could be measured also by other methods, such as using electron spin resonance and fluorescence probes [3], and the viscosity change corresponding to the capability of

moving of fatty acyl chains in the membrane was detected as a kinetic parameter of microenvironment of the probes. On the other hand, the measurement of membrane fluidity by infrared spectroscopy may show the extent of packing of membrane acyl chains, or in another words "softness of the membrane" which is a static parameter of macroenvironment.

Actually, the change of membrane fluidity may be measured by the change of infrared absorption peak position for methylene CH symmetric stretching mode at around 2850 cm^{-1} [1,2] as well as NMR measurement [4]. In the fluidity measurement, the peak shift to lower wave number direction indicated that the membrane became harder or ordered in the lipid network structure, whereas the shift to higher wave number direction indicated softer or disordered [5]. The infrared spectroscopic analysis could be used for elucidation of phase behavior of long-chain phospholipid membranes [2].

In lipid bilayer membranes, acyl chains in the lipids are interacted with each other by the van der Waals or London forces. When the interaction among methylenes was increased with the increase of packing of the membrane acyl chains which were attracted with each other by London forces, methylene CH bond force constant might be decreased. This would shift the CH symmetric stretching mode-originated infrared absorption peak to the lower wave number (energy) direction, for example, a shift from 2853 to 2852 cm^{-1}, indicating hardening of the membrane and usually observed when the temperature was decreased from 37 to 10 °C for pig brain microsomal membranes (unpublished result).

In another case, the Fourier-transform infrared (FTIR) spectroscopic analysis of lipid O=P=O, C=O, and C–H vibrational bands of POPC/CHOL (palmitoleic phosphatidylcholine/cholesterol mixture) liposomes revealed an increase in the conformational order of the acyl chains at or close to the predicted critical cholesterol molar fractions [3]. Here, the shift of methylene infrared absorption peak was observed from 2851.2 to 2850.7 cm^{-1} when the fraction of cholesterol was increased from 0% to 40%. This indicated that the insertion of cholesterol to POPC model membrane contributed to the increase of packing of membrane acyl chains.

For measurement of membrane fluidity in the biological tissues such as artery, it would be difficult to use probe methods (using fluorescence anisotropy measurement and electron spin resonance spectroscopy) because the probe methods would require the insertion of external probe to the tissue membranes and the suitable insertion of probe might be practically impossible to the arterial membrane. Infrared spectroscopy provides a technique that does not require the insertion of probes, and this is especially advantageous for measurement of biological tissues.

Actually, the application of FTIR for measurement of mouse pulmonary artery was reported [6] and the change of conformational disorder (fluidity) in the artery membrane lipids could be detected. In this case, the arterial

tissue was sandwiched by CaF_2 disks and the transmission FTIR absorption spectrum could be measured. In this report, the average conformational disorder in membrane lipids in the pulmonary artery *in situ* was increased by the treatment of monocrotaline which was a toxic alkaloid and caused early pulmonary endothelial injury with gradual development of pulmonary hypertension. Moreover, the membrane fluidity of carotid tissue of spontaneously hypertensive rat could also be measured *in situ* [7], and the membrane fluidity was increased in the hypertensive rat carotid subjected to anoxia, but not in the control rat. In the carotid or pulmonary arterial tissues, the increase of membrane conformational disorder would be linked to vulnerability of the tissue membrane.

2.2. Hydration of Membrane

The state of hydration of membrane surface may affect the hydrolytic activity in or on the surface of membrane, and the hydration may be closely related to the presence of glycans on the membrane, especially glycosylated lipids and proteins. Actually, it was reported that the interfacial properties of cell membranes were important and phospholipase A_2 activity was influenced by hydration (or in another word, water activity) of the membrane surface [8–10], and thus the inflammation was affected.

Hydration state around carboxyl and phosphate groups may be affected by the presence of polyhydroxy compounds (such as glycans) or by changing the chemical groups esterified to the phosphates, mainly choline, ethanolamine, or glycerol. Thus, surface membrane properties, such as the dipole potential and the surface pressure, are modulated by the water at the interphase region by changing the structure of the membrane components [10–13].

The hydration or dehydration of membrane surface could be measured by FTIR using the absorption of hydroxy (–OH) and carboxylate (–COO–) groups which would be changed by the change of hydrogen bonding with water around the residues on the membrane surface. It was reported previously [8] that nondestructive FTIR analysis could detect the modification of rat brain microsomal membranes and these modifications of brain microsomal membranes were dependent on the dietary fatty acids and learning behavior. In this report [8], FTIR spectral differences for brain microsomes were observed mainly in the absorption bands of fatty acyl ester at around 1730 cm^{-1} (*sn*-2 position), phosphate ester and oligosaccharides in the range of 1050–1100 cm^{-1}. The infrared band of fatty acyl ester at the *sn*-2 position in the microsomal membrane shifted to a higher wave number position (1731 cm^{-1}) in the perilla oil-diet group (α-linolenic acid-rich) than that in the safflower oil group (α-linolenic acid-deficient) at 1727 cm^{-1} after the learning behavior, suggesting a difference between both groups in hydrogen bonding of the fatty acyl ester with water. Without learning behavior, both groups showed similar ester absorption at *sn*-2 position (1729

and 1728 cm^{-1}). The infrared band shift observed for the *sn*-2 ester was interpreted to be mainly due to the change of hydrogen bonding strength between the *sn*-2 fatty ester (C=O) and the surrounding water molecules.

2.3. Microdomain Structure of Membrane

It has been reported that the normal cell membranes may contain microdomains which may play various roles in cell functions such as intracellular trafficking, signal transduction, and cell–cell recognition [14,15], and the FTIR spectroscopy could show the presence of microdomains in cell membranes [16]. This microdomain has been named sometimes as "raft" or "nanoclusters" [17,18].

A report [16] showed that the membrane assemblies in the liquid crystalline phase were prepared and then the membrane dispersions were rapidly cooled to induce the gel phase where lateral diffusion was dramatically inhibited, and the lipid microdomains were found by FTIR and ultrasonic velocimetry to be in a nanometer size in scale, in contrast to the micron-sized domains more commonly found in phase-separated systems [19,20]. Here, methylene (in perdeuterated DPPC-d_{62}; dipalmitoylphosphatidylcholine) infrared absorption at around 1090 cm^{-1} for CD_2 methylene deformation (bending) band was split at −120 °C with a splitting of 8.1 ± 0.2 cm^{-1}, and the CH_2 deformation (bending) mode at around 1470 cm^{-1} of GalCer (galactocerebroside) and DPPC mixture also showed splitting at −120 °C.

In this report, the CH_2 deformation mode existed as a single peak at 1469 cm^{-1} at 20 °C but was split in a manner similar to that of the pure GalCer dispersion at −120 °C. Two separate splitting parameters in the second derivative spectrum were observed. The inner splitting, 2.2 ± 0.8 cm^{-1}, corresponded to the sphingosine chain, whereas the outer splitting of the stearoyl chain was 7.0 ± 0.1 cm^{-1}. This outer splitting for GalCer in the DPPC-d_{62} bilayer matrix corresponded to approximately six chains. DPPC-d_{62} also evinced a temperature-dependent change, representative of microdomain formation. The microdomains in the membrane may have different fluidity or viscosity from the other region of the membrane, and thus the methylene infrared absorption band would be different.

2.4. Protein–Lipid Interactions

Protein–lipid interaction may play a key role in the function of cell membranes, and several methods were applied to detect the interactions, and the FTIR was one of those methods [21,22].

A report [23] showed that FTIR spectroscopy indicated the presence of interaction of P_γ (heterotrimeric G protein γ-subunit peptide) and P_γ-FN

(the farnesylated peptide) with the polar and interfacial regions of phospholipid bilayers. The binding of P_γ-FN to model membranes was due to the farnesyl group and positively charged amino acids near this lipid. On the other hand, membrane lipids partially altered P_γ-FN structure, in turn increasing the fluidity of phospholipid membranes. These data highlight the relevance of the interaction of the C-terminal region of the G_γ (G protein γ-subunit) protein with the cell membrane and its effect on membrane structure. In this report, 1,2-dielaidoyl-*sn*-glycero-3-phospho-ethanolamine (DEPE) and 1,2-dimyristoyl-*sn*-glycero-3-phosphate sodium salt (DMPA) were used as the membrane lipids.

In this report, P_γ-FN and P_γ exhibited an amide I band characteristic of β-sheet structures with maxima at 1625 (P_γ-FN) or 1638 (P_γ) cm^{-1} and a weak component at around 1688 cm^{-1}. Amide I spectra of both peptides also displayed a random-coil component with a shoulder at around 1645–1649 cm^{-1}. A centrifugation assay was used to analyze the membrane binding of both peptides qualitatively under the conditions used in FTIR experiments. The band at 1625 cm^{-1} was more prominent in the presence of DEPE and even more so in the presence of DMPA, indicating an increase in the proportion of P_γ-FN that adopts a β-sheet structure as a result of its association with DEPE or DMPA lipids. In the case of the P_γ peptide and in the presence of DMPA membranes, the amide I band was observed in the membrane pellet. The spectra of P_γ in DEPE membranes showed two main bands at 1652 and 1633 cm^{-1}, which clearly differed from the FTIR spectrum of P_γ alone. This might indicate that the association of the peptide with DEPE bilayers induced a partial loss of the β-sheet secondary structure, adopting α-helical and/or random-coil structures.

As shown in this report typically, the membrane lipids may affect the secondary structure of membrane proteins and peptides, and this structural change may cause functional changes of the proteins [24,25]. On the other hand, *vise versa*, the membrane structures may be changed by the presence of peptides and hydrophobic proteins [26,27]. These changes of protein–lipid interactions were well detected by FTIR when the experiment was suitably designed.

3. Membrane Lipids and Fatty Acids in Human Tissues

For human tissues, the measurements of proteins, glycans, lipids, and fatty acids by infrared spectroscopy were frequently performed to investigate the link between the diseases and the changes of tissue/cell compositions and characters [28–30].

Diseases of human—such as cancer, diabetes, and cardiovascular diseases—may have various aspects of tissue/cell structural and functional changes, and these diseases may accompany many molecular and signal network changes. Some cancers may include an increase in the nuclei-to-cytoplasm ratio, increase of the relative amount of DNA, enhancement of the phosphorylation of proteins, a decrease in the glycogen level, a loss of hydrogen bonding of the C–OH groups in the amino acid residues of proteins, a decrease in the overall CH_3-to-CH_2 ratio, and an accumulation of triglycerides [28]. The most significant merit in using FTIR for measurement or diagnosis of these tissue/cell changes is that FTIR may be able to detect these changes of biomolecular functional groups simultaneously and noninvasively by one shot of measurement.

3.1. Cancer Tissues

Initially, the application of FTIR to the study of cancers was performed by Rigas's group [28] in 1990, and human colorectal cancers displayed abnormal FTIR spectra. It was reported that all cancer specimens displayed abnormal spectra compared with the corresponding normal tissues, involving the changes in the phosphate and CO stretching bands, the CH stretch region, and the pressure dependence of the CH_2 bending and C=O stretching modes. It may be interesting to note that in malignant colonic tissue, the intensity of methyl (CH_3) band at 2958.5 cm^{-1} was decreased while that of the symmetric methylene (CH_2) band at 2852.5 cm^{-1} was increased, when compared with the corresponding bands in normal tissue. This indicated that the ratio of the number of methyl groups to that of methylene groups was decreased in malignant tissues, compared with normal colonic tissue, indicating that the lipids or fatty acids were relatively increased in the colonic cancer tissue. In this report, the pressure dependence of the CH_2 bending mode at around 1470 cm^{-1} was also measured to investigate the packing characteristics of methylene chains in the membrane lipids. At atmospheric pressure, the frequency of this band was higher in the malignant tissue than that in its normal counterpart, and this relationship was reversed as pressure increased.

Normally, colorectal cancer comes in many forms and main form is adenocarcinoma. Rigas and Wong [29] reported in another paper that the pressure dependence of the frequency of the CH_2 bending mode at around 1470 cm^{-1} had been used to study interchain packing and order/disorder properties of lipid bilayers, and the pressure dependence of the mode for HCT15 adenocarcinoma cell line was very close to that displayed by normal colon tissues. This indicated one of two possibilities that either this property was not critical to malignant transformation or the cultured colonocytes had dispensed with such a requirement.

Recently, the FTIR spectroscopic studies for cancer cells of esophagus [31] and viral cancer progression of cervical tissues [32] were reported.

Maziak and Wong's group [31] reported in 2007 that specific changes were observed in the FTIR spectral features of esophageal cancer, including a *decrease* in the overall CH_3-to-CH_2 ratio and an accumulation of triglycerides, an enhancement in the phosphorylation of proteins, and so on. On the other hand, Bogomolny and Huleihel's group [32] pointed out that the infection of murine sarcoma virus to murine fibroblast cell lines (NIH/3T3) and mouse embryonic fibroblast (MEF) cells progressed malignancy in those cells and cervical tissues and the protein/lipid ratios (CH_3-to-CH_2 ratio) were *increased* in the progressed cancer cells and tissues, and this is a contradictory result against the Rigas's group data [29,30] where CH_3-to-CH_2 ratios were decreased in the colon and esophageal cancer cells. These results may indicate that the change of lipid metabolism in cancer cells, that is, whether the accumulation of triglyceride occurred or not, may be dependent on the cancer cell types.

3.2. Fatty Acid Metabolism and Metabolic Diseases

Epidemiological research using fatty acid compositional analyses of human body fluids (blood, etc.) and tissues may be important for assessment of the effectiveness of dietary fatty acids on the physiology of the human body. However, the measurement of fatty acid compositions in tissues involves tedious and time-consuming procedures for extraction and derivatization (methyl ester, etc.) of fatty acids from tissues for subsequent analyses with gas chromatography or high-performance liquid chromatography. These standard chromatographic methods may not be practically suitable for a large-scale epidemiological research. On the other hand, vibrational spectroscopies such as Raman and infrared spectroscopies may be useful techniques to measure lipid compositions in food staffs and human tissues and fluids. It has been reported that nondestructive FTIR–ATR measurement of human oral mucosa [33] could monitor diurnal changes of polyunsaturated fatty acids in the mucosa. On the other hand, Lam *et al.* [34] also reported that FTIR and chemometrics revealed low-density lipoprotein oxidation with protein conformational changes and provided a simple rapid technique for measuring primary and secondary oxidation products.

Furthermore, the fatty acid compositions of human oral mucosa could be measured using FTIR–ATR method [33,35]. In this report, the second derivative infrared spectra of the mucosal tissues in the wave number regions from 1600 to 1760 cm^{-1} and 2800 to 3050 cm^{-1} were analyzed with PLS multivariate regression analysis method. The predicted values were compared with the measured values of 10 categorized fatty acid compositions, that is, a (saturated C17 or lower), b(C16:1 + C17:1), c(C18:0), d(C18:1), e(C18:2), f(saturated C20 or longer), g(C20:3 + C20:4), h(C22:1 + C24:1), i(C22:6), and j(γC18:3), where γC18:3 is γ-linolenic acid. Almost all fatty acid compositions of oral mucosa were well predicted with difference between predicted

and measured values within ±5% of total; however, errors were relatively larger in minor components such as C22:6 than major components.

Many papers have been published concerning multivariate analysis methods for fatty acid compositional analyses [36–38] using vibrational spectroscopy. Beattie *et al.* [36] reported that the bulk unsaturation parameters and abundance of polyunsaturated fatty acids of several adipose tissues could be predicted by Raman spectroscopy using multivariate analysis. They reported that Raman analysis has the advantage of giving good correlation coefficients without the need for prior solvent extraction steps in the analysis. On the other hand, Ripoche and Guillard [37] reported when using FTIR that the prediction of fatty acid composition of unextracted adipose tissue gave poor correlation coefficient ($R^2 = 0.69$–0.79). Improvement of the coefficient in the reported case [33] may result mainly from using less noisy second derivative infrared spectra in the selected wave number regions. Afseth *et al.* [38] reported using Raman and near-IR spectroscopic methods that Raman spectroscopy was suitable for predicting the total level of unsaturation, and both Raman and near-IR spectroscopy were feasible for rapid quantification of fat composition in complex food model systems.

Moreover, it was reported that FTIR–ATR technique could monitor the metabolism of docosahexaenoic acid in the adult body *in situ* and noninvasively [39]. Normally, the ingested lipids in foods were digested and adsorbed through intestine to blood and to liver, and resorbed through vessels to peripheral tissues, including skin tissues. It may be essential to find out sites of human body, especially skin tissues, where the lipid and fatty acid changes of blood were reflected nearly immediately, to measure noninvasively with FTIR–ATR. In this chapter, the change of human lip surface lipid compositions reflected well that of ingested lipids, and the changes of lipids and fatty acids were really detected with FTIR–ATR *in situ*. Human lip has generally four portions anatomically (1) appendage-bearing epidermis, (2) keratinized vermilion (red zone), (3) parakeratinized intermediate zone, and (4) labial mucosal epithelium. Yoshida *et al.* [39] measured the lower lip, that is, keratinized vermilion surface (outermost stratified corneum) by FTIR–ATR method, and this portion was suitable to measure the metabolism of polyunsaturated fatty acids originated from diet.

Diabetes mellitus is one of the metabolic diseases, and normally the diagnosis of diabetes is usually done by using the measurement of blood glucose and hemoglobin A1c, a glycosylated protein. Recently, it was reported [40] that the FTIR spectral analysis revealed differences in several major metabolic components—lipids, proteins, glucose, thiocyanate, and carboxylate—that clearly demarcated healthy and diseased saliva. In this report, differences in Fourier self-deconvolution processed mean IR spectra were noted from normal and diabetic saliva, and the difference spectrum helped identify molecular components most at variance between two groups of spectra. For example, the lipid ester band at 1735 cm^{-1} was

more intense in the diabetic saliva, while the bands located at 1400 and 1582 cm^{-1}—the symmetric and asymmetric carboxyl radical stretching vibrations of carboxylate groups such as those in lactate or side chains of protein in saliva—were decreased for diabetic saliva. The role of lactate in the modulation of hormone release and responsiveness and in the control of homeostasis was recently reviewed by Sola-Penna [41]. Another spectral area including 950–1180 cm^{-1} for C–C/C–O stretch of sugar moieties and 1020 cm^{-1} for C–O of glycogen was contributed from AGEs (advanced glycation end products) of diabetic saliva.

Even very recently, a number of reports have appeared concerning to the application of infrared spectroscopy to measurement of biomolecules including lipids of human tissues and cells nondestructively [42–51], and these reports may indicate that the infrared spectroscopy or vibrational spectroscopy has been increasingly recognized to be useful for clinical diagnosis of human diseases.

4. Skin and Hair Lipids and Membranes

The structure and function of lipids and membranes in skin surface tissues, that is, stratum corneum (SC) and hairs, were quite different from those in other normal organs, such as liver and heart tissues. These differences may be realized by the very special roles of skin SC and hairs, and both SC and hairs are integrated cells without living. Even though these tissues are not alive, they really play a protective and important role for the body, and the integrity of those "dead cells" is indispensable for the functions. Lipids and their interactions with proteins are especially important for the integrity of cells and matrix and for the barrier function of those tissues. In this section, we show data obtained mainly from our laboratory.

Figure 1 shows the FTIR–ATR spectra of human face skin (stratum corneum) in the two zones: U3 (the chin skin) and T1 (the forehead skin). This suggested that T1 skin SC contained more lipids than U3 skin SC. It was also noted that the fingerprint areas (1000–1400 cm^{-1}) in both zones were significantly different in the IR spectra.

Figure 2 shows the FTIR–ATR spectra of human hairs, outer and inner surfaces, measured by microscopic FTIR measurement system. The inner surface showed a clear peak at around 3010 cm^{-1}.

4.1. Protein-Bound Fatty Acid and Ceramides in Hairs

Human scalp hairs are comprised of proteins (>90% in dry weight) and lipids (<10%) and those components provide hair fibers with suitable elasticity and mechanical resistance against elongation and torsion. Hair lipids [52] are mainly composed of squalene, wax esters, triacylglycerol,

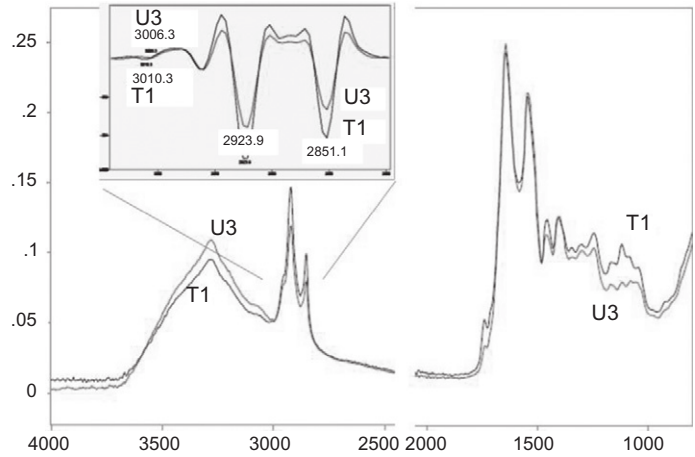

Figure 1 FTIR–ATR spectra of human face skin in T1 and U3 zones.

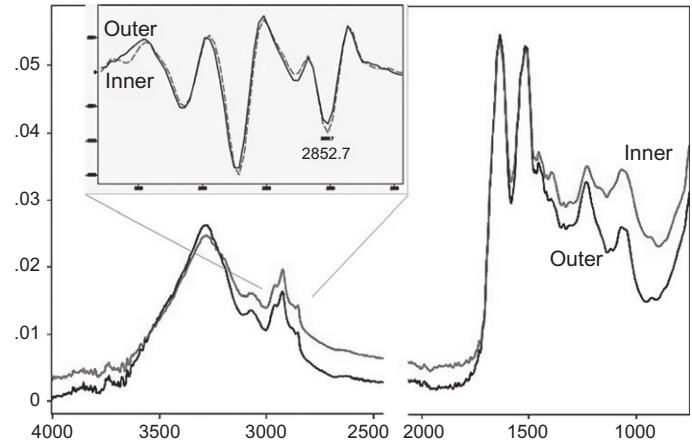

Figure 2 FTIR–ATR spectra of human hairs, outer and inner surfaces. Inserted are the second derivative spectra at around 3010 cm^{-1} and 3000–2800 cm^{-1} regions for CH stretching vibration of *cis*-unsaturated C–C bonds and methylene/methyl CH vibrations, respectively.

free fatty acids, cholesterol, ceramides, cholesterol sulfate, 18-methyl-eicosanoic acid (18-MEA), and other minor components.

Among these lipids, only 18-MEA binds covalently to the cuticle surface proteins with a thioester linkage. 18-MEA is known as a specially designed branched-chain fatty acid and makes the hair surface hydrophobic and acts as a boundary lubricant to decrease friction resistance with providing a large segmental volume of the anteiso-moiety which exhibit liquid phase-like behavior on the hair cuticle [53].

18-MEA could be detected normally by gas chromatography after removal from hair proteins with saponification. The measurement of hair cuticle surface by FTIR–ATR may detect 18-MEA as a major branched-chain fatty acid. As shown in Fig. 2, the FTIR spectra of hair outer and inner surfaces indicated that the methylene CH symmetric stretching mode was observed at 2852.7 cm^{-1}, which was a little higher wave number position than that of skin methylene mode observed at 2851.1 cm^{-1} (Fig. 1). Here, the inner surface was prepared by cutting a hair fiber in the middle with a microplane. Figure 2 also suggested that unsaturated fatty acids were much less in the outer surface of cuticle than the inner surface of hair because the outer surface did not show clear IR absorbance at around 3010 cm^{-1} (originated from CH stretch of *cis*-CH=CH double bond) whereas the inner surface had a clear absorbance at around 3010 cm^{-1}. These results indicated that the phase of 18-MEA bundles on the cuticle surface was in more fluid or disordered state than skin surface, and these data were consistent with the idea that the anteiso-moiety of 18-MEA exhibited liquid-like behavior. The relatively disordered state of 18-MEA may be resulted from the presence of 18-methyl branch in the fatty acyl chain, but not from the unsaturated bonds in acyl chains which were practically absent on the surface of hair cuticle.

Ceramides are contained in human hairs as well as skin, and especially nonhydroxy or α-hydroxy fatty acid moiety and a dihydrosphingosine moiety are thought to be present in hair CERs. It has been hypothesized that the CERs were related to apoptosis during keratinization in living hair matrix cells to dead cuticular or cortical cells and contributed to barrier function and water holding in hair. It was reported [54] that the composition of CERs in hair was characterized by predominant CERs with saturated or unsaturated and carbon even-numbered fatty acid moieties and C18 dihydrosphingosine moiety, and also by isomeric CERs, α-hydroxy fatty acid-containing CERs, and odd chain-containing CERs.

As shown in Fig. 2, the IR absorption intensity of amide II (at around 1550 cm^{-1}) or amine-derived band (at around 3300 cm^{-1}) or NH bending/stretching and C–N stretching mode was relatively higher in hair than in skin (Fig. 1), and this may indicate the mixing of IR spectra of amide-related band of various CERs which had various hydroxy forms and various peak positions at 1535–1560 cm^{-1} [55]. So far, there is no report which showed that the CERs in hair or skin were directly observed *in situ* by FTIR–ATR, but somehow the amide bands in FTIR of hair or skin may be affected by the presence of CERs.

4.2. Minor Lipids in Hair

As described earlier, major lipids in hair medulla are squalene, wax esters, triacylglycerols, free fatty acids, cholesterol, ceramides, and cholesterol sulfate. 18-MEA is present on the cuticle. We found also minor lipids

present in the whole hair shaft, and also in hair bulb (root) as described below. Figure 3A shows the silica gel–TLC pattern of the hair extracted lipids (developed with chloroform:methanol (95:12) solvent mixture), and the minor component is circled on the figure and is called "lipid X" here. The "lipid X" extracted from the silica gel plate was dissolved in methanol and measured by FTIR shown in Fig. 3A (right). This IR spectrum clearly indicated the presence of amide bond in the lipid X compound, and also fatty acyl (at around 2850 cm^{-1}) and glycan (at around 1050 cm^{-1}) structures. The ESI-MS spectrum of this compound (lipid X) was compared with the standard esterified sterylglucoside (ESG) as shown in Fig. 3B because lipid X was developed very near to the position of ESG in the TLC (Fig. 3A, left). The ESI-MS patterns were similar with each other; however, mass peak positions were different. Especially, the widely distributed fine peaks cluster at around m/z 910 (± 60) was found in the standard ESG with constant mass peak gas of $\Delta 16$ mu, and that at around m/z 840 (± 70) was in the lipid X compound with various mass peak gaps of $\Delta 12$, $\Delta 14$, $\Delta 24$, and $\Delta 26$ mu. Further analysis of the compound was done after acidic hydrolysis and the materials in aqueous phase were observed with ESI-MS method as shown in Fig. 3C.

In Fig. 3C, ESI-MS spectra of the standard acetylated glucose and acetylated *N*-acetylglucosamine (GlcNAc) were presented (upper panel), and the mass pattern of acetylated materials of the hydrolyzed and extracted "lipid X" compound in aqueous phase was also presented (lower panel). When both acetylated GlcNAc and acetylated soluble "lipid X" fragments were compared, the ESI-MS patterns of both were almost identical. Acetylated glucose was also observed, and these results suggested that lipid X composed of GlcNAc and glucose as glycan structures. We observed that cholesterol and lanosterol were contained in the hydrophobic fraction of hydrolyzed lipid X compound (not shown in this section), and summarized the candidate structures of the ESG-like compound (lipid X) in Fig. 3D. All mass patterns could be reasonably explained by the combination of various fatty acids and glucose or GlcNAc, and cholesterol or lanosterol. As GlcNAc contains amide bond in the structure, this mass spectral result was consistent with the previous FTIR data which suggested the presence of amide bond in lipid X.

On the other hand, hair bulb obtained from hairs naturally removed was investigated by FTIR and mass analysis for the extracted lipids from the hair bulb. In Fig. 3E, a microphoto of a typical hair bulb was shown after cut off from the shaft. We could detect IR spectra at the hair bulb top (root side), middle, and the site near shaft separately by FTIR–ATR with microscope (IlluminatIR; SmithDetection, Inc., UAS). Normally, the IR spectrum of hair shaft surface was different from that of hair bulb or root especially in the IR absorption intensity at 1395 cm^{-1}, and this IR absorption was much higher in bulb than in hair shaft surface. Even within the bulb, the peak ratios between

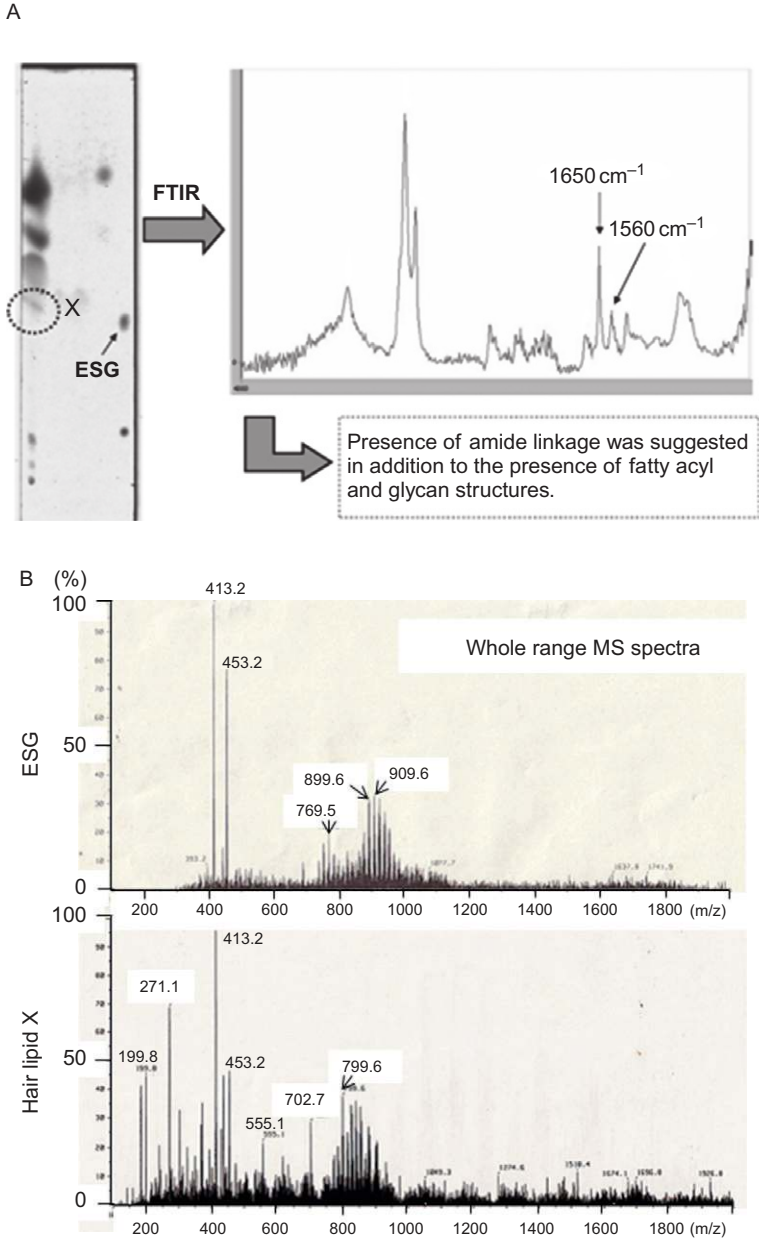

Figure 3 (Continued)

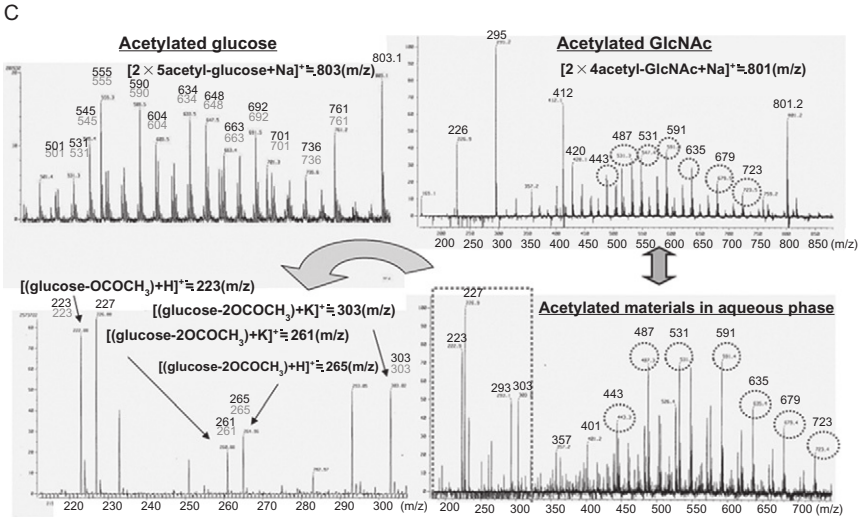

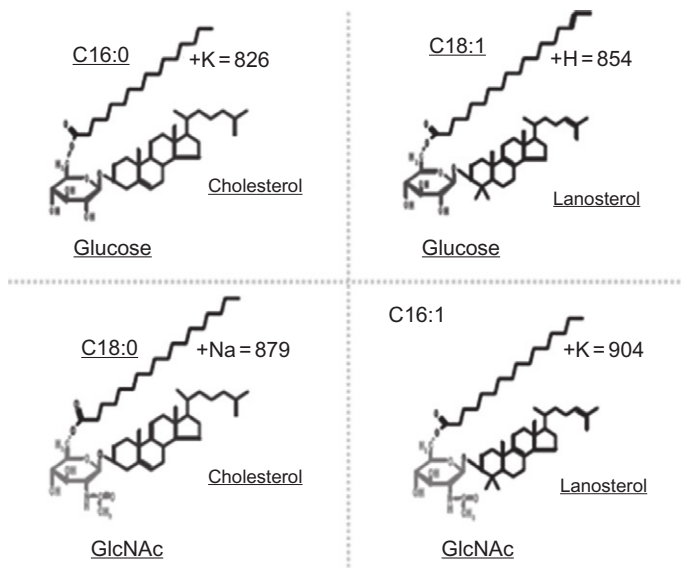

Figure 3 (Continued)

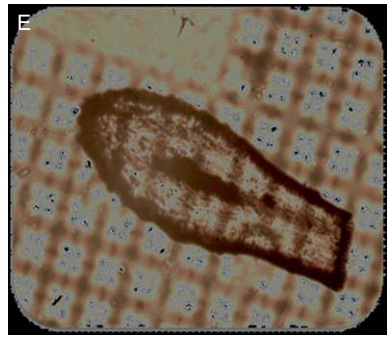

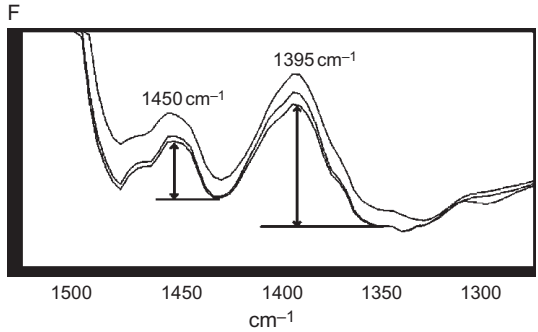

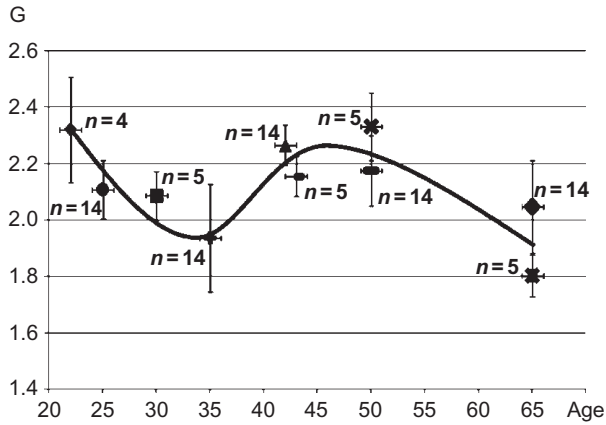

Figure 3 (Continued)

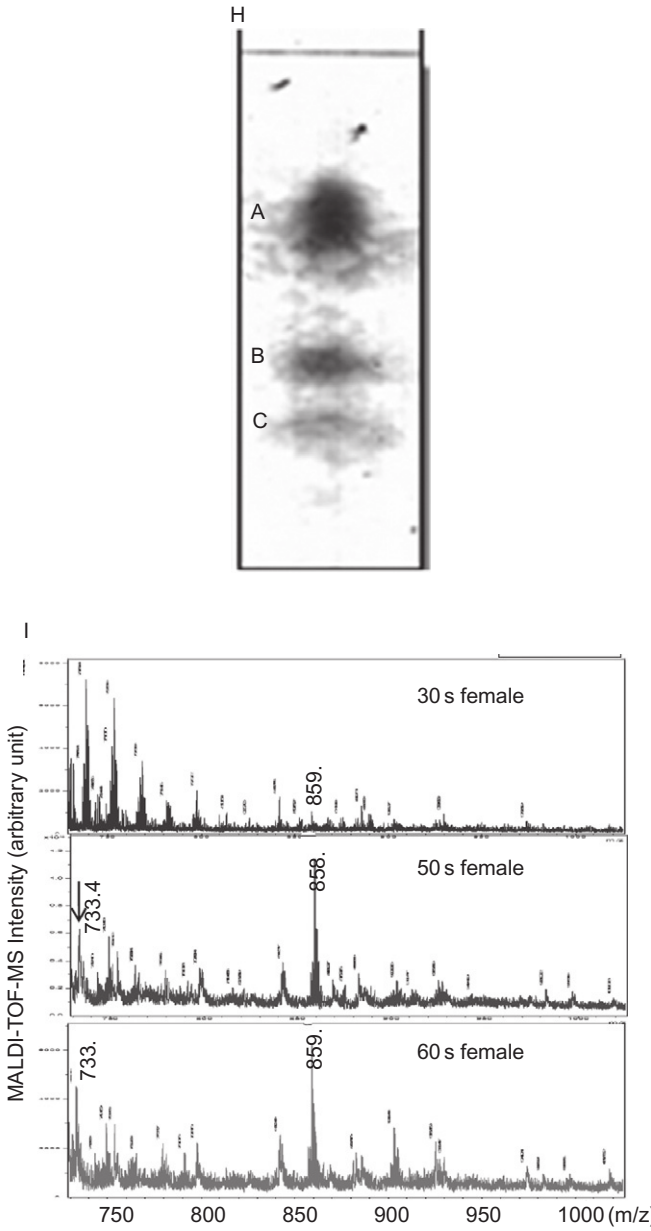

Figure 3 (A) Ester sterylglycoside-like lipids in human hair shaft detected by TLC and FTIR. Left: the silica gel–TLC patterns of the hair extracted lipids. Right: FTIR spectrum of "lipid X." (B) ESI–MS spectra of ester sterylglucoside (standard) and "lipid X." (C) ESI–MS spectra of saccharides in aqueous phase in ester

(1395 cm^{-1}) and (1450 cm^{-1}) were different among these sites, and the ratio was higher at the bulb top (root side) than the site near shaft (Fig. 3F).

The age-dependent changes of the ratio at the middle of the bulb were shown in Fig. 3G. The subjects from whom the hairs were collected were all women from 20s to 60s of ages (*n* was the number of hair bulbs measured). This figure indicated that the ratio became smaller in 30s of age, and again increased in 40s and 50s, then decreased again in 60s. The hair bulb component which showed a typical IR absorption at 1395 cm^{-1} may be regulated in the age-dependent manner, and probably by hormone.

We had revealed that the 1395 cm^{-1} component in the hair bulb was a lipid-like material, and the typical TLC pattern of extracted lipids from the bulb was shown in Fig. 3H. This pattern was obtained in the silica gel plate with chloroform/methanol (95:12) as a development solvent which was used for hair shaft extract shown in Fig. 3A.

In Fig. 3H, the spot A contained main neutral lipids such as squalene and triglycerides and spot B may contain free cholesterol. The spot C was supposed to contain free fatty acids (FFAs) and ceramides (CERs) and other minor components, and ESG-like compound found in hair shaft may also be contained in spot C. The relative spot intensity of spot C as the ratio of spot C to spot A showed the age dependencies, and the intensity of spot C was the lowest for 30s of age and higher in 40s–60s of ages (not shown in this section).

The components of spot C were analyzed by MALDI-TOF-MS spectrometry (with 2,5-dihydroxybenzoic acid as a matrix) after extraction from the silica gel. We found mass peaks which showed the lowest for the spot C extract of 30s of age and higher for 40s–60s of ages, and those peaks were at *m/z* 858–859 as shown in Fig. 3I. Normally, in MALDI-TOF-MS spectrometry, free fatty acids (mainly C16–C18) and ceramides may show mass peaks below *m/z* 700 (typically *m/z* 500–650 for ceramides), and a peak at *m/z* 733 may represent a reduced form of C16:0 sphingomyelin. The mass peaks at *m/z* 858–859 were in the range typically observed for ESGs as shown in Fig. 3A–D.

However, fatty acyl ESGs had no strong IR absorption at around 1390 cm^{-1}, so it may be reasonable to assume that the hair bulb-specific component with IR absorption at 1395 cm^{-1} might be the modified fatty acyl ESG, and it has been known that typical IR absorption at 1390–1400 cm^{-1} was originated from nitrated compound (modified by NO_2),

sterylglucoside-like lipids. Acetylated glucose and acetylated N-acetylglucosamine were used as standards. (D) Candidates of esterified sterol glycolipids in human hair shaft. (E) A typical microphotograph of a hair bulb after cutting off from the shaft. (F) FTIR spectra of hair shaft surface and bulb at around 1400 cm^{-1}. (G) Age-dependent changes of FTIR peak ratios between (1395 cm^{-1}) and (1450 cm^{-1}) at the middle of bulbs. (H) A typical TLC pattern of extracted lipids from the bulb. (I) Age-dependent MALDI-TOF-MS profiles for esterified sterylglucoside in spot C of (H).

and actually the synthesized nitro-lanosterol compound in our laboratory showed IR band at around 1390 cm^{-1} (not shown in this section).

Finally, we assumed that the compound in hair bulb (in spot C of Fig. 3H) which had IR absorption at 1395 cm^{-1} and the mass peak at around m/z 859 might be the nitrated compound with glucose + cholesterol + C18:1, which showed calculated molecular mass at m/z 859.2, as a candidate.

4.3. Effect of Dietary Lipids on the Hair Lipids

Hair lipids and fatty acids may be supplied originally from dietary lipids and thus from blood, and metabolized in hair follicle to synthesize hair-specific components, such as type I and II hair keratin proteins, 18-MEA fatty acid, and various lipids including ceramides and sterol glycosides. However, direct relationship has not been demonstrated between dietary lipid intake and the storage of lipids in hair fibers so far, and here we show a part of data suggesting the correlation between dietary fat intake and appearance of lipids in hair.

Figure 4 indicates the method to measure FTIR spectrum of one hair fiber with FTIR–ATR spectroscopy with microscope (IlluminatIR; Smith-Detection, Inc., USA), and the right inserted photo showed the scale (110 μm) and actual hair fiber. The measurement of half-cut hair fiber surface was done by attaching the ATR probe on the points marked in Fig. 4 (left) with 110 μm intervals.

In Fig. 5A, the scanning electron micrograph of half-cut hair was demonstrated, and many fine fibers were present. Figure 5B showed the presence of periodic changes of relative IR intensities at 2960 cm^{-1} in the direction along longitudinal axis of hair fiber for four subjects (two men and two women), and the fine periodicity (point-to-point period was nearly 8 h) was averaged to obtain one point as the 1-week-averaged data. Roughly, the length (0.33 mm) containing three points would correspond to nearly 24 h as the scalp hairs are thought to grow with normally 0.3–0.4 mm long a day.

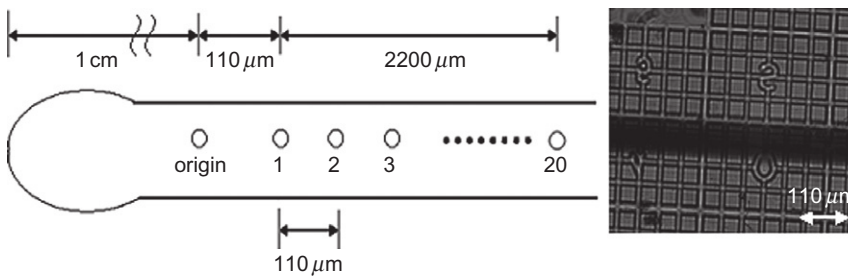

Figure 4 Illustration of the method to measure FTIR spectrum of one hair fiber with FTIR–ATR spectroscopy with microscope.

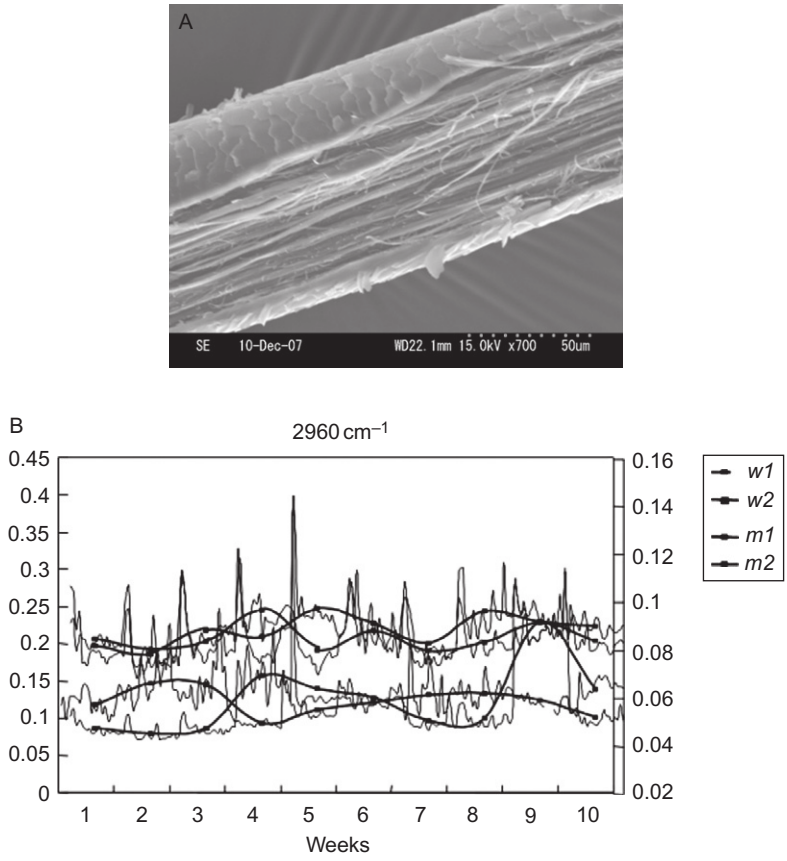

Figure 5 (A) A scanning electron micrograph of half-cut hair. (B) The periodic changes of relative IR intensities at 2960 cm^{-1} in the direction along longitudinal axis of hair fibers for four subjects.

The collection of naturally lost hairs once a week and the FTIR measurement of medulla surface at the fixed position of the hairs may detect time-dependent changes of hair molecules. Figure 6A and B showed time-dependent changes of IR absorption intensities at around 2855 cm^{-1} and changes of dietary total lipids intake which were calculated from the daily-food intake questionnaire with FFQg program (Food Frequency Questionnaire Based on Food Groups in Japan; http://www.kenpakusha.co.jp/), respectively. Then one could search the time gap between the date of lipid intake and the date of appearance of lipids in the hair with higher correlation by changing the time-gap step by step.

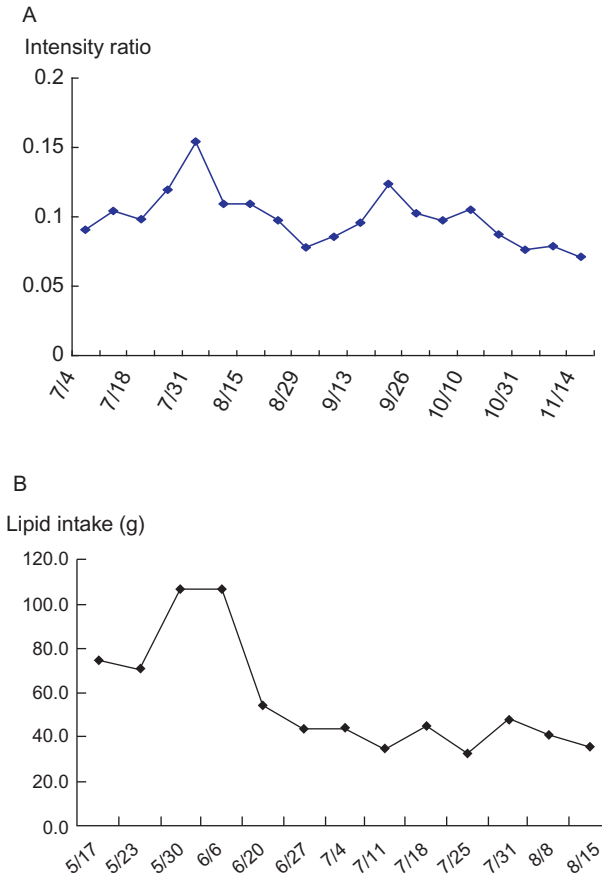

Figure 6 (A) Time-dependent changes of IR absorption intensities at around 2855 cm^{-1}. (B) Time-dependent changes of dietary total lipids intake.

Figure 7 shows the highest correlated case between the hair lipid ratio in FTIR and the amount of lipid intake with significant correlated coefficient ($r = 0.88$), which was found by step-by-step validation, and actually in this case the time gap was 11 weeks.

In Table 1, the summarized data were presented for four male subjects and the corresponding time gaps were nearly 10 or 17 weeks. Interestingly, the negative correlations were also observed for two cases, and this suggested that the accumulation of lipids into hair was observed 10 or 16 weeks later after the intake of lipids on the one hand, and the removal of lipids from hair might be observed on the other hand. In the latter case, the accumulation of lipids may occur in the visceral fat or subcutaneous fat mainly, and the other accumulation in hair or other peripheral tissues may

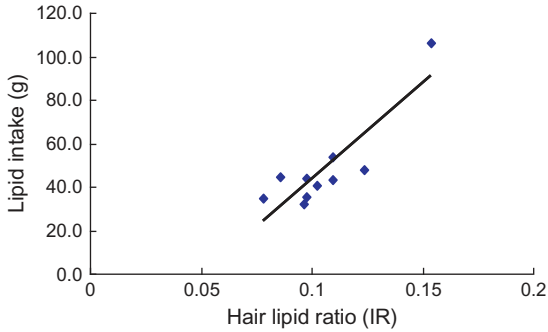

Figure 7 Correlation between the hair lipid ratio in FTIR and the amount of dietary lipid intake.

Table 1 The highest correlation coefficients between the hair lipid ratio in FTIR and the amount of lipid intake for four subjects with the corresponding time gaps

Subject no.	Correlation coefficient (r)	Highly correlated time-gap correspondent (weeks)
1	0.68	8–11
2	0.88	8–11
	0.88	15–18
3	−0.86	15–18
4	−0.73	7–9

be suppressed. Actually, the subject no. 3 and 4 showed the negative correlation and also high body fat values which were independently measured by the electric current sensor (Tanita Co., Japan). Human hair growth cycle was thought to contain normally 6–8 weeks of catagen and telogen phases without hair cell growth and the incorporation of lipids in hair may be regulated only in the anagen (growth) phase. Then, the 10-weeks gap between the date of lipid intake and the calculated date of appearance in the hair may suggest that the measured point in the hair, nearly 10 mm apart from the hair root top, corresponded roughly to 4 weeks, and nearly 6 weeks of catagen and telogen phases may be the resting period and then the hair was naturally released from the scalp skin.

4.4. *In Situ* Measurements of Skin Surface Molecules

The barrier function of the skin is mainly provided by the SC, where CERs, CHOL, and FFAs are present mainly and the lipids in SC form highly ordered crystalline lamellae phase. These lamellae are crucial for a proper skin barrier function. FTIR spectroscopy was used to examine the lipid

organization of mixtures prepared from synthetic CERs with CHOL and FFAs. A report [56] showed that conformational ordering and lateral packing of these mixtures indicated great similarities to the lipid organization in SC and lipid mixtures prepared with native CERs. In SC, the number of hydroxy (OH) groups in the head groups of CER subclasses varied. Acyl CERs with a linoleic acid chemically bound to a long acyl chain were also identified. This report revealed that CER head group architecture affected the lateral packing and conformational ordering of the CER:CHOL:FFA mixtures. Furthermore, while the majority of the lipids formed a crystalline packing, the linoleate moiety of the acyl CERs participated in a "pseudo-fluid" phase.

Recently, the other report [55] showed that the FTIR spectroscopic systematic study revealed the hydrated SC lipid barrier model systems composed of an equimolar mixture of a ceramide, free palmitic acid, and cholesterol. The mixing properties with cholesterol and palmitic acid were considered by using perdeuterated palmitic acid and proteated ceramides. Both molecules could be monitored separately using mid-infrared spectroscopy. At physiological relevant temperatures, between 30 and 35 °C, orthorhombic as well as hexagonal chain packing of the ceramide molecules was observed. The formation of chain packing was dependent on lipid hydration, with a decrease in ceramide hydration favoring the formation of orthorhombic hydrocarbon chain packing, as well as temperature. The investigated SC mixtures exhibited a rich polymorphism from crystalline domains with heterogeneous lipid composition to a "fluid" homogeneous phase. The study showed that under physiological conditions (pH 5.5, hydrated, 30–35 °C) of the skin ternary systems composed of an equimolar ratio of ceramides, free palmitic acid and cholesterol might form gel-like domains delimitated by a liquid-crystalline phase boundary. The presented results supported the microstructural arrangement of the SC lipids as suggested by the "domain mosaic model."

The function of skin SC may be basically regulated by not only lipids, but also other biomolecules and those interactions. Especially, hydrophilic biomolecules in SC are playing important roles in maintaining the barrier function.

Lactic acid is a major α-hydroxy acid in natural moisturizer factor (NMF) and found in SC and also in sweat. It was reported recently that the lactic acid and its compound on SC could be monitored noninvasively by FTIR [57], and this report presented that *in situ* and noninvasive measurement of FTIR spectra of human face surface could detect the circa-monthly rhythmic change of the components which included mainly the mixture of magnesium (Mg)–lactate complex and other skin surface soluble components. It was reported that 12% of lactic acid existed in NMF in the skin, and functioned as a part of moisturizer factor in SC. Lactic acid is normally produced in the glycolytic reactions in the tissue cells through reduction of pyruvate with NADH via lactate dehydrogenase (LDH). Thus,

the amount of lactic acid may be controlled by changing LDH activity and the amount of NADH and other glucose metabolites in the energy metabolism in human cells. On the other hand, acidic mucopolysaccharides or sulfated glycosaminoglycans (GAGs) play important roles in the extracellular matrix of skin tissues, and these include keratan sulfate and dermatan sulfate. The sulfated GAGs had a sulfate-derived FTIR absorption normally at 1200–1250 cm^{-1} originated from S=O stretching mode [58], and actually a peak at 1243 cm^{-1} could be observed in the component with circa-monthly changes of intensity in the outermost layer of the face skin. On the other hand, the water extract of T1-face skin contained negatively charged fraction (named as Fraction X) in HPLC with a strong anion-exchange column, and this fraction after dried showed FTIR spectrum with broad bands at 1100–1200 cm^{-1}, not clear peak at 1230–1250 cm^{-1}, and this IR absorption pattern was very similar to the IR spectrum of acidic magnesium salt of proteoglycan aggregates [59]. The IR absorption of S=O stretching mode could be largely affected by ionic conditions, especially by binding of a divalent cation with sulfate group. In line with these data, it was suggested that the Fraction X might contain partly magnesium (or calcium)-bound glycosaminoglycan sulfate.

From our present results, Mg–lactate and the aforementioned divalent cation (Mg^{2+})-bound GAGs may play important roles in the circa-monthly rhythmic changes of human skin SC.

In the maintenance and control of formation and exfoliation of skin SC, the activity of protease (cathepsin D) in SC against transglutaminase was reported to play an important role [60]. The turnover of the skin surface cells was reported to have about 4–5 weeks of period [61]. It was reported that in the SC, the endoglycosidase activity of heparanase 1 might be indispensable and represented the first step in the desquamation process [62], and so the degradation of heparan sulfate polymers into shorter chains may be concerned to the exfoliation of SC.

5. Future Perspectives and Conclusion

Infrared spectroscopy, or vibrational spectroscopy, may have a great potential in the application to diagnosis of human diseases. So far, we reviewed mainly the application of mid-infrared spectroscopy to biological cells and tissues, especially the measurements of membranes and lipids and other related biomolecules of human disease-related tissues. Other vibrational spectroscopies, such as near-infrared absorption and Raman scattering spectroscopies, are also important and developing techniques for diagnosis of human diseases, and many applications to biological tissues and cells have been reported.

All these vibrational spectroscopic techniques may have the advantage in measuring changes of biofactors related to diseases as described in this chapter, and many factors including proteins, lipids, glycans, and even other unknown materials may be detected in one shot of experiment, and moreover the interaction among these biofactors in the membranes may also be detected by vibrational spectroscopy. Especially, the latter case is important for the diagnosis of complex human diseases because many factors are actually involved and these factors are more or less connected in the onset of diseases, such as cancer, atherosclerosis, and diabetes mellitus. For example, lowering of LDL–cholesterol in human enhanced the expression of *cyclooxygenase 2* gene in arterial wall and platelet, and changed the inflammation status with changing the production of prostaglandins [63] and thus affected many metabolic status of lipids and other related biomolecules. Changing of one factor would change the state of the other factors and this is the change of metabolic network, and so this network is the target of metabolomics study. This is because the metabolomics study is attracting many medical researches for diagnosis and medical treatment or therapy of diseases.

Vibrational spectroscopies may reveal *nondestructively* and *in situ* the changes of property and quantity of biomolecules of human tissues *in vivo*. Especially for diagnosis of human diseases, the measurement of human skin including lip surface or other easily accessible tissues *in vivo* may be important as skin surface (stratum corneum), may be refreshed nearly every day, and reflects somehow the chemical and biological states of inner tissues which was theoretically and presumably at the stage where cell components were affected several weeks ago depending upon the skin keratinocyte turnover rate. The skin SC may thus contain information about biomolecules including proteins, lipids, and glycans which may be affected several weeks ago in the dermis by the compositions of blood, and especially the diseases such as diabetes and hyper- (or hypo-) lipidemia may change more or less the character of skin biomolecules.

The lipids and membrane structures and functions of human skin SC may be very special, and they play not only the protective role or barrier for human body, but also the regulatory role for reabsorption of exogenous materials such as sweat and sebum components or medicines or other chemicals. The development of more effective drug delivery system through skin tissues (transdermal therapeutic system) may be important in the present and future medical treatments. Infrared spectroscopy, especially FTIR–ATR, could be applied to investigate the mechanism of transdermal transport of chemicals and the enhancer of transport [64,65]. Other vibrational spectroscopic methods like the confocal laser Raman scattering spectroscopic method could also be applied to the skin and transdermal transport research [66].

If the vibrational spectroscopy could be used and handled very easily and precisely to measure the change of biomolecules with sophisticated chemometric methods, it would take the place of the usual clinical tests, especially for screening of diseases, and for this purpose more technical innovations may be needed in the development of infrared spectroscopic machinery specifically for diagnosis of human diseases. The infrared spectroscopic innovations, if succeeded, would result in not only the innovation of clinical screening of human diseases, but also the advancement of realization of the basic metabolic mechanisms of lipids and their interaction with proteins and glycans in human tissues *in vivo*, and after that we would get for the first time the real techniques to monitor physiological molecular dynamics in human.

ACKNOWLEDGMENTS

We thank Dr. S. Sakuyama (Mandom Co., Japan) for help in the skin works. We appreciate the collaboration of many students who carried out many experiments and helped us considerably, namely H. Inukai, Y. Tanaka, T. Yonebayashi, K. Morita, T. Futamura, A. Hayashi, C. Hirabayashi, S. Matsushima, M. Ishibashi, T. Nakata, and M. Yoshida for recent hair and skin works, and Bitoh, Kanai, Kanebayashi, Kayugawa, Miyake, Nakano, and Sugiura for previous hair works. We also thank Mr. H. Tanamachi and Dr. Y. Masukawa (Kao Co., Japan) for their help to write this chapter. We thank Dr. R. Nakayama (Kyoto Women's University) for providing FFQg program. These works were financially supported in part by Grants-in-Aid for Scientific Research from Ministry of Education, Science, Sports, and Culture of Japan to S.Y., and also by Kao Co., Japan. We thank sincerely Dr. Yoshinori Muto (Gifu University) for providing us the chance to write this chapter.

REFERENCES

[1] R.G. Snyder, H.L. Strauss, C.A. Elliger, Carbon-hydrogen stretching modes and the structure of *n*-alkyl chains. 1. Long, disordered chains, J. Phys. Chem. 86(26) (1982) 5145–5150.
[2] R.G. Snyder, G.L. Liang, H.L. Strauss, R. Mendelsohn, IR spectroscopic study of the structure and phase behavior of long-chain diacylphosphatidylcholines in the gel state, Biophys. J. 71(6) (1996) 3186–3198.
[3] B. Cannon, G. Heath, J. Huang, P. Somerharju, J.A. Virtanen, K.H. Cheng, Time-resolved fluorescence and Fourier transform infrared spectroscopic investigations of lateral packing defects and superlattice domains in compositionally uniform cholesterol/phosphatidylcholine bilayers, Biophys. J. 84(6) (2003) 3777–3791.
[4] V.R. Kodati, M. Lafleur, Comparison between orientational and conformational orders in fluid lipid bilayers, Biophys. J. 64(1) (1993) 163–170.
[5] M. Fidorra, L. Duelund, C. Leidy, A.C. Simonsen, L.A. Bagatolli, Absence of fluid-ordered/fluid-disordered phase coexistence in ceramide/POPC mixtures containing cholesterol, Biophys. J. 90(12) (2006) 4437–4451.
[6] S. Yoshida, M. Miyata, H. Yoshida, M. Takeshita, Change of conformational disorder in membrane lipids in the pulmonary artery of monocrotaline-injected rats detected in situ by Fourier transform infrared spectroscopy, Vib. Spectrosc. 3(4) (1992) 271–276.

[7] S. Yoshida, N. Makino, M. Takeshita, Effect of anoxia on carotid of spontaneously hypertensive rat: studies by scanning electron microscopy and Fourier transform infrared spectroscopy, J. Clin. Biochem. Nutr. 8 (1990) 41–50.
[8] S. Yoshida, M. Miyazaki, K. Sakai, M. Takeshita, S. Yuasa, A. Sato, et al. Fourier transform infrared spectroscopic analysis of rat brain microsomal membranes modified by dietary fatty acids: possible correlation with altered learning behavior, Biospectroscopy 3(4) (1997) 281–290.
[9] C.S. Rao, S. Damodaran, Surface pressure dependence of phospholipase A2 activity in lipid monolayers is linked to interfacial water activity, Colloids Surf. B Biointerfaces 34(3) (2004) 197–204.
[10] E.A. Disalvo, F. Lairion, F. Martini, E. Tymczyszyn, M. Frias, H. Almaleck, et al. Structural and functional properties of hydration and confined water in membrane interfaces, Biochim. Biophys. Acta 1778(12) (2008) 2655–2670.
[11] M.C. Luzardo, F. Amalfa, A.M. Nunez, S. Diaz, A.C. Biondi De Lopez, E.A. Disalvo, Effect of trehalose and sucrose on the hydration and dipole potential of lipid bilayers, Biophys. J. 78(5) (2000) 2452–2458.
[12] J.H. Crowe, L.M. Crowe, D. Chapman, Infrared spectroscopic studies on interactions of water and carbohydrates with a biological membrane, Arch. Biochem. Biophys. 232 (1) (1984) 400–407.
[13] J.V. Ricker, N.M. Tsvetkova, W.F. Wolkers, C. Leidy, F. Tablin, M. Longo, et al. Trehalose maintains phase separation in an air-dried binary lipid mixture, Biophys. J. 84(5) (2003) 3045–3051.
[14] D.A. Brown, E. London, Functions of lipid rafts in biological membranes, Annu. Rev. Cell Dev. Biol. 14 (1998) 111–136.
[15] G. Vereb, J. Szollosi, J. Matko, P. Nagy, T. Farkas, L. Vigh, et al. Dynamic, yet structured: the cell membrane three decades after the Singer–Nicolson model, Proc. Natl. Acad. Sci. USA 100(14) (2003) 8053–8058.
[16] Z.D. Schultz, I.W. Levin, Lipid microdomain formation: characterization by infrared spectroscopy and ultrasonic velocimetry, Biophys. J. 94(8) (2008) 3104–3114.
[17] M. Edidin, The state of lipid rafts: from model membranes to cells, Annu. Rev. Biophys. Biomol. Struct. 32 (2003) 257–283.
[18] S.J. Plowman, C. Muncke, R.G. Parton, J.F. Hancock, H-ras, K-ras, and inner plasma membrane raft proteins operate in nanoclusters with differential dependence on the actin cytoskeleton, Proc. Natl. Acad. Sci. USA 102(43) (2005) 15500–15505.
[19] E. London, How principles of domain formation in model membranes may explain ambiguities concerning lipid raft formation in cells, Biochim. Biophys. Acta 1746 (3) (2005) 203–220.
[20] J.R. Silvius, Partitioning of membrane molecules between raft and non-raft domains: insights from model-membrane studies, Biochim. Biophys. Acta 1746(3) (2005) 193–202.
[21] A. Bhushan, M.G. McNamee, Differential scanning calorimetry and Fourier transform infrared analysis of lipid–protein interactions involving the nicotinic acetylcholine receptor, Biochim. Biophys. Acta 1027(1) (1990) 93–101.
[22] D. Dorn-Zachertz, G. Zimmer, Different protein–lipid interaction in human red blood cell membrane of Rh positive and Rh negative blood compared with Rhnull, Z. Naturforsch. C 36(11–12) (1981) 988–996.
[23] F. Barcelo, J. Prades, J.A. Encinar, S.S. Funari, O. Vogler, J.M. Gonzalez-Ros, et al. Interaction of the C-terminal region of the Ggamma protein with model membranes, Biophys. J. 93(7) (2007) 2530–2541.
[24] Y.P. Zhang, R.N. Lewis, R.S. Hodges, R.N. McElhaney, Peptide models of the helical hydrophobic transmembrane segments of membrane proteins: interactions of acetyl-K2-(LA)12-K2-amide with phosphatidylethanolamine bilayer membranes, Biochemistry 40(2) (2001) 474–482.

[25] M. Gasset, J.M. Mancheno, J. Lacadena, A. Martinez del Pozo, M. Onaderra, J.G. Gavilanes, Spectroscopic characterization of the alkylated alpha-sarcin cytotoxin: analysis of the structural requirements for the protein–lipid bilayer hydrophobic interaction, Biochim. Biophys. Acta 1252(1) (1995) 43–52.
[26] I.J. Vereyken, V. Chupin, F.A. Hoekstra, S.C. Smeekens, B. de Kruijff, The effect of fructan on membrane lipid organization and dynamics in the dry state, Biophys. J. 84 (6) (2003) 3759–3766.
[27] N.M. Tsvetkova, I. Horvath, Z. Torok, W.F. Wolkers, Z. Balogi, N. Shigapova, et al. Small heat-shock proteins regulate membrane lipid polymorphism, Proc. Natl. Acad. Sci. USA 99(21) (2002) 13504–13509.
[28] B. Rigas, S. Morgello, I.S. Goldman, P.T. Wong, Human colorectal cancers display abnormal Fourier-transform infrared spectra, Proc. Natl. Acad. Sci. USA 87(20) (1990) 8140–8144.
[29] B. Rigas, P.T. Wong, Human colon adenocarcinoma cell lines display infrared spectroscopic features of malignant colon tissues, Cancer Res. 52(1) (1992) 84–88.
[30] M.A. Cohenford, B. Rigas, Cytologically normal cells from neoplastic cervical samples display extensive structural abnormalities on IR spectroscopy: implications for tumor biology, Proc. Natl. Acad. Sci. USA 95(26) (1998) 15327–15332.
[31] D.E. Maziak, M.T. Do, F.M. Shamji, S.R. Sundaresan, D.G. Perkins, P.T. Wong, Fourier-transform infrared spectroscopic study of characteristic molecular structure in cancer cells of esophagus: an exploratory study, Cancer Detect. Prev. 31(3) (2007) 244–253.
[32] E. Bogomolny, S. Argov, S. Mordechai, M. Huleihel, Monitoring of viral cancer progression using FTIR microscopy: a comparative study of intact cells and tissues, Biochim. Biophys. Acta 1780(9) (2008) 1038–1046.
[33] S. Yoshida, Y. Okazaki, T. Yamashita, H. Ueda, R. Ghadimi, A. Hosono, et al. Analysis of human oral mucosa ex vivo for fatty acid compositions using Fourier-transform infrared spectroscopy, Lipids 43(4) (2008) 361–372.
[34] H.S. Lam, A. Proctor, J. Nyalala, M.D. Morris, W.G. Smith, Quantitative determination of low density lipoprotein oxidation by FTIR and chemometric analysis, Lipids 39(7) (2004) 687–692.
[35] S. Yoshida, H. Yoshida, Noninvasive analyses of polyunsaturated fatty acids in human oral mucosa in vivo by Fourier-transform infrared spectroscopy, Biopolymers 74 (5) (2004) 403–412.
[36] J.R. Beattie, S.E. Bell, C. Borgaard, A. Fearon, B.W. Moss, Prediction of adipose tissue composition using Raman spectroscopy: average properties and individual fatty acids, Lipids 41(3) (2006) 287–294.
[37] A. Ripoche, A.S. Guillard, Determination of fatty acid composition of pork fat by Fourier transform infrared spectroscopy, Meat Sci. 58(3) (2001) 299–304.
[38] N.K. Afseth, V.H. Segtnan, B.J. Marquardt, J.P. Wold, Raman and near-infrared spectroscopy for quantification of fat composition in a complex food model system, Appl. Spectrosc. 59(11) (2005) 1324–1332.
[39] S. Yoshida, Q.Z. Zhang, S. Sakuyama, S. Matsushima, Metabolism of fatty acids and lipid hydroperoxides in human body monitoring with Fourier transform infrared spectroscopy, Lipids Health Dis. 8 (2009) 28.
[40] D.A. Scott, D.E. Renaud, S. Krishnasamy, P. Meric, N. Buduneli, S. Cetinkalp, et al. Diabetes-related molecular signatures in infrared spectra of human saliva, Diabetol. Metab. Syndr. 2 (2010) 48.
[41] M. Sola-Penna, Metabolic regulation by lactate, IUBMB Life 60(9) (2008) 605–608.
[42] M.A. Mackanos, C.H. Contag, Fiber-optic probes enable cancer detection with FTIR spectroscopy, Trends Biotechnol. 28(6) (2010) 317–323.

[43] A. Beljebbar, S. Dukic, N. Amharref, M. Manfait, Screening of biochemical/histological changes associated to C6 glioma tumor development by FTIR/PCA imaging, Analyst 135(5) (2010) 1090–1097.
[44] M.J. Baker, C. Clarke, D. Demoulin, J.M. Nicholson, F.M. Lyng, H.J. Byrne, et al. An investigation of the RWPE prostate derived family of cell lines using FTIR spectroscopy, Analyst 135(5) (2010) 887–894.
[45] V.W. Petit, M. Refregiers, C. Guettier, F. Jamme, K. Sebanayakam, A. Brunelle, et al. Multimodal spectroscopy combining time-of-flight-secondary ion mass spectrometry, synchrotron-FT-IR, and synchrotron-UV microspectroscopies on the same tissue section, Anal. Chem. 82(9) (2010) 3963–3968.
[46] A. Zwielly, S. Mordechai, I. Sinielnikov, A. Salman, E. Bogomolny, S. Argov, Advanced statistical techniques applied to comprehensive FTIR spectra on human colonic tissues, Med. Phys. 37(3) (2010) 1047–1055.
[47] Y. Tuo, P. Huang, Y. Ke, S. Fan, Q. Lu, B. Xin, et al. Attenuated total reflection Fourier transform infrared spectroscopic investigation of the postmortem metabolic process in rat and human kidney cortex, Appl. Spectrosc. 64(3) (2010) 268–274.
[48] L. Zhang, A. Aksan, Fourier transform infrared analysis of the thermal modification of human cornea tissue during conductive keratoplasty, Appl. Spectrosc. 64(1) (2010) 23–29.
[49] M.A. Mackanos, C.H. Contag, FTIR microspectroscopy for improved prostate cancer diagnosis, Trends Biotechnol. 27(12) (2009) 661–663.
[50] U. Zelig, J. Kapelushnik, R. Moreh, S. Mordechai, I. Nathan, Diagnosis of cell death by means of infrared spectroscopy, Biophys. J. 97(7) (2009) 2107–2114.
[51] K. Belbachir, R. Noreen, G. Gouspillou, C. Petibois, Collagen types analysis and differentiation by FTIR spectroscopy, Anal. Bioanal. Chem. 395(3) (2009) 829–837.
[52] Y. Masukawa, H. Narita, G. Imokawa, Characterization of the lipid composition at the proximal root regions of human hair, J. Cosmet. Sci. 56(1) (2005) 1–16.
[53] Y. Masukawa, H. Tsujimura, H. Tanamachi, H. Narita, G. Imokawa, Damage to human hair caused by repeated bleaching combined with daily weathering during daily life activities, Exog. Dermatol. 3(6) (2004) 273–281.
[54] Y. Masukawa, H. Tsujimura, H. Narita, Liquid chromatography-mass spectrometry for comprehensive profiling of ceramide molecules in human hair, J. Lipid Res. 47 (7) (2006) 1559–1571.
[55] P. Garidel, B. Fölting, I. Schaller, A. Kerth, The microstructure of the stratum corneum lipid barrier: mid-infrared spectroscopic studies of hydrated ceramide:palmitic acid:cholesterol model systems, Biophys. Chem. 150(1–3) (2010) 144–156.
[56] M. Janssens, G.S. Gooris, J.A. Bouwstra, Infrared spectroscopy studies of mixtures prepared with synthetic ceramides varying in head group architecture: coexistence of liquid and crystalline phases, Biochim. Biophys. Acta 1788(3) (2009) 732–742.
[57] S. Sakuyama, C. Hirabayashi, J. Hasegawa, S. Yoshida, Analysis of human face skin surface molecules in situ by Fourier-transform infrared spectroscopy, Skin Res. Technol. 16(2) (2010) 151–160.
[58] M.O. Longas, K.O. Breitweiser, Sulfate composition of glycosaminoglycans determined by infrared spectroscopy, Anal. Biochem. 192(1) (1991) 193–196.
[59] S.M. Bychkov, V.N. Bogatov, S.A. Kuz'mina, Analysis of the salts of cartilage proteoglycan aggregates, Biull. Eksp. Biol. Med. 94(11) (1982) 52–55.
[60] F. Egberts, M. Heinrich, J.M. Jensen, S. Winoto-Morbach, S. Pfeiffer, M. Wickel, et al. Cathepsin D is involved in the regulation of transglutaminase 1 and epidermal differentiation, J. Cell Sci. 117(Pt. 11) (2004) 2295–2307.
[61] G. Lindwall, E.A. Hsieh, L.M. Misell, C.M. Chai, S.M. Turner, M.K. Hellerstein, Heavy water labeling of keratin as a non-invasive biomarker of skin turnover in vivo in rodents and humans, J. Invest. Dermatol. 126(4) (2006) 841–848.

[62] D. Bernard, B. Mehul, C. Delattre, L. Simonetti, A. Thomas-Collignon, R. Schmidt, Purification and characterization of the endoglycosidase heparanase 1 from human plantar stratum corneum: a key enzyme in epidermal physiology? J. Invest. Dermatol. 117(5) (2001) 1266–1273.
[63] L.H. Smith, M.S. Petrie, J.D. Morrow, J.A. Oates, D.E. Vaughan, The sterol response element binding protein regulates cyclooxygenase-2 gene expression in endothelial cells, J. Lipid Res. 46(5) (2005) 862–871.
[64] E. Touitou, V.M. Meidan, E. Horwitz, Methods for quantitative determination of drug localized in the skin, J. Control. Release 56(1–3) (1998) 7–21.
[65] Y. Obata, S. Utsumi, H. Watanabe, M. Suda, Y. Tokudome, M. Otsuka, et al. Infrared spectroscopic study of lipid interaction in stratum corneum treated with transdermal absorption enhancers, Int. J. Pharm. 389(1–2) (2010) 18–23.
[66] N. Nakagawa, M. Matsumoto, S. Sakai, In vivo measurement of the water content in the dermis by confocal Raman spectroscopy, Skin Res. Technol. 16(2) (2010) 137–141.